

Article

Bioinspired Mineralization of Type I Collagen Fibrils with Apatite in Presence of Citrate and Europium Ions

Jaime Gómez–Morales ^{*,1} , Raquel Fernández Penas ¹, Cristóbal Verdugo-Escamilla ¹, Lorenzo Degli Esposti ^{2,3} , Francesca Oltolina ⁴, Maria Prat ⁴ , Michele Iafisco ² and Jorge Fernando Fernández Sánchez ⁵

¹ Laboratorio de Estudios Cristalográficos, IACT, CSIC–UGR. Avda. Las Palmeras, n° 4. E–18100 Armilla (Granada), Spain; raquel@lec.csic.es (R.F.P.); cristobal.verdugo@csic.es (C.V.E.)

² Institute of Science and Technology for Ceramics (ISTEC), National Research Council (CNR), Via Granarolo 64, 48018 Faenza (RA), Italy; lorenzo.degliesti@istec.cnr.it (L.D.E.); michele.iafisco@istec.cnr.it (M.I.)

³ Department of Chemistry, Life Sciences and Environmental Sustainability, University of Parma, Parco Area delle Scienze 11/a, 43124 Parma, Italy

⁴ Department of Health Sciences, Università del Piemonte Orientale A. Avogadro, via Solaroli 17, 28100 Novara, Italy; francesca.oltolina@med.uniupo.it (F.O.); maria.prat@med.uniupo.it (M.P.)

⁵ Department of Analytical Chemistry, Faculty of Sciences, University of Granada, Avda. Fuentenueva s/n, 18071 Granada, Spain; jffernan@ugr.es

* Correspondence: jaime@lec.csic.es; Tel.: +34-958-230000; Ext. 190203

Received: 24 October 2018; Accepted: 21 December 2018; Published: 25 December 2018



Abstract: Synthetic nanostructured hybrid composites based on collagen and nanocrystalline apatites are interesting materials for the generation of scaffolds for bone tissue engineering. In this work, mineralized collagen fibrils were prepared in the presence of citrate and Eu^{3+} . Citrate is an indispensable and essential structural/functional component of bone. Eu^{3+} endows the mineralized fibrils of the necessary luminescent features to be potentially employed as a diagnostic tool in biomedical applications. The assembly and mineralization of collagen were performed by the neutralization method, which consists in adding dropwise a $\text{Ca}(\text{OH})_2$ solution to a H_3PO_4 solution containing the dispersed type I collagen until neutralization. In the absence of citrate, the resultant collagen fibrils were mineralized with nanocrystalline apatites. When citrate was added in the titrant solution in a Citrate/Ca molar ratio of 2 or 1, it acted as an inhibitor of the transformation of amorphous calcium phosphate (ACP) to nanocrystalline apatite. The addition of Eu^{3+} and citrate in the same titrant solution lead to the formation of Eu^{3+} -doped citrate-coated ACP/collagen fibrils. Interestingly, the relative luminescent intensity and luminescence lifetime of this latter composite were superior to those of Eu^{3+} -doped apatite/collagen prepared in absence of citrate. The cytocompatibility tests, evaluated by the 3-(4,5-Dimethylthiazol-2-yl)-2,5-diphenyltetrazolium bromide (MTT) colorimetric assay in a dose-dependent manner on GTL–16 human gastric carcinoma cells, on MG–63 human osteosarcoma cells and on the m17.ASC, a spontaneously immortalized mouse mesenchymal stem cell clone from subcutaneous adipose tissue, show that, in general, all samples are highly cytocompatible.

Keywords: collagen mineralization; apatite; amorphous calcium phosphate; citrate; europium; luminescence; cytocompatibility

1. Introduction

The hierarchically-structured architecture of human mineralized tissues such as bones and teeth has long fascinated scientists and engineers, and a considerable effort has been devoted to produce synthetic materials inspired from the natural ones [1]. The replication of the natural

mineralized tissues is a big challenge for materials scientists because they are formed *in vivo* through biomineralization processes that involve cascades of complex events such as self-assembly, mineralization and self-organization [2].

The basic building block of bone tissue structure is a self-assembled collagen fibril (mainly type I collagen) mineralized with oriented apatite nanocrystals at both intrafibrillar and interfibrillar zones [3–6]. Type I collagen is a trimeric molecule consisting of two $\alpha 1$ and one $\alpha 2$ peptide chains that comprise a repeating Gly(glycine)–X–Y sequence, with X and Y being usually proline and hydroxyproline residues. The collagen molecules self-assemble under physiological conditions into triple helical structures forming the so-called tropocollagen. The interaction between tropocollagen units leads to self-organization into fibrillar structures having a regular array of holes and overlap zones that can be observed by transmission electron microscopy (TEM) as a periodic banding pattern of 67 nm [7,8]. The apatite component in bone is different from stoichiometric hydroxyapatite [$\text{Ca}_{10}(\text{PO}_4)_6(\text{OH})_2$], namely it is calcium- (and hydroxide-) deficient and doped with 4–6 wt % of carbonate, 0.9 wt % of Na, 0.5 wt % of Mg and others minor elements [9]. The apatite nanoparticles are poorly crystalline and display a typical plate-like morphology favoring the peculiar mechanical properties of bone [10–12]. Recently, Hu et al. [13] using nuclear magnetic resonance (^{13}C -NMR) have revealed that citrate accounts for about 5.5 wt % of total organic matrix of bone and it is strongly bound to the surface of the apatite nanoparticles (1 molecule/2 nm²). Its presence and abundance should not be considered adventitious but would reflect an important role in the biomineralization process [13,14]; therefore, the study of the effect of citrate in the formation of biomimetic apatite nanoplatelets as well as in collagen mineralization has become a subject of intense research in the last years [15–19]. The last results have shown that the use of citrate is an interesting and straightforward nature inspired strategy to control the chemical-physical features of the apatite for the development of improved nanoparticle-based biomaterials [20–22].

Nanostructured hybrid composites based on collagen and nanocrystalline apatites synthesized with bio-inspired processes are widely used as scaffolds in bone tissue engineering because, thanks to the analogy with the natural bone tissue, they are able to activate the molecular mechanisms of regeneration and repair, and they can be absorbed and replaced by the newly formed tissue [22–24]. Although their regenerative potential is no matter of discussion, several synthetic strategies could be employed to enhance their biological activities and wide their applications. For example, the use of citrate as additive in the preparation of apatite/collagen composites could improve the biological performances of these devices because it can increase their similarity with the natural tissue. Recent works have also suggested that citrate is an indispensable and essential structural/functional component of bone and dental tissue [16,25]. In addition, the incorporation of luminescent features in the scaffolds would be of high value for certain biomedical applications such as the monitoring of tissue regeneration at the early stages by medical imaging or its use as diagnostic tool. In this respect, the preparation of apatite nanocrystals in presence of citrate and Eu^{3+} , with tailored luminescent properties, was already reported [26].

In this work, in a first step, hybrid collagen/apatite fibrils were prepared both in absence and in presence of citrate to analyze the effect of this small molecule on the chemical-physical features of the composites. Subsequently, Eu^{3+} was added to generate luminescent composites potentially able to act as diagnostic tool in bone tissue engineering. Eu^{3+} was selected because its ionic radius (0.95 Å) is close to that of Ca^{2+} (0.99 Å); this could enable an effective substitution of Eu^{3+} in the Ca^{2+} sites of the apatitic part of the composite. Compared to other rare-earth elements, Eu^{3+} has a simple electronic energy level scheme and hypersensitive transitions [27]. In addition, *in vitro* biological tests have revealed the lack of toxicity and good cytocompatibility of ceramic materials doped with small amounts of Eu^{3+} [28].

2. Materials and Methods

2.1. Materials

Type I collagen extracted from equine tendon was purchased from OPOCRIN Spa (Corlo di Formigine, MO, Italy). Calcium hydroxide ($\text{Ca}(\text{OH})_2$, ≥ 96.0 pure) was provided by Fluka. Orthophosphoric acid (H_3PO_4 , ACS reagent, $\geq 85\%$ in H_2O), europium chloride hexahydrate ($\text{EuCl}_3 \cdot 6\text{H}_2\text{O}$, ACS Reagent, 99.9% pure) and sodium citrate tribasic dihydrate ($\text{Na}_3\text{cit} \cdot 2\text{H}_2\text{O}$) where cit = citrate = $\text{C}_6\text{H}_5\text{O}_7$, ACS reagent, $\geq 99.0\%$ pure) were provided by Sigma–Aldrich. All solutions were prepared with ultrapure water ($0.22 \mu\text{S}$, 25°C , Milli–Q, Millipore).

2.2. Assembly and Mineralization of Collagen

The assembly and mineralization of collagen was performed by the neutralization method as previously reported [29,30]. Briefly, a solution of composition $0.495 \text{ M Ca}(\text{OH})_2$ was added dropwise to $10 \text{ mL } 0.290 \text{ M H}_3\text{PO}_4$ solution containing 500 mg of dispersed type I collagen until reaching a pH value close to neutrality (a, blank experiment, Col/Ap). The first set of experiments was aimed to study the influence of citrate ions in the preparation of the Col/Ap composites. In this respect two different citrate concentrations were tested and the basic solution contained either (b) $0.495 \text{ M Ca}(\text{OH})_2 + 0.990 \text{ M Na}_3\text{cit}$, cit_{high}–Col/Ap) or (c) $0.495 \text{ M Ca}(\text{OH})_2 + 0.495 \text{ M Na}_3\text{cit}$ (cit_{low}–Col/Ap). Besides that, the addition of (d) $0.990 \text{ M Na}_3\text{cit}$ solution in the reaction vessel just after the neutralization reaction (Col/Ap–cit_{high}) was also evaluated. The second set of experiments was designed to prepare luminescent Col/Ap fibrils by adding Eu^{3+} . The acidic solution was titrated by adding dropwise either a basic solution of composition (e) $0.495 \text{ M Ca}(\text{OH})_2 + 0.990 \text{ M Na}_3\text{cit} + 0.010 \text{ M EuCl}_3$ (cit_{high}–Eu/Col/Ap) or (f) $0.495 \text{ M Ca}(\text{OH})_2 + 0.010 \text{ M EuCl}_3$ (Eu/Col/Ap). In all experiments the suspensions were magnetically stirred for 2 hours at 25°C , then sieved ($50 \mu\text{m}$ mesh), washed 3 times by centrifugation at 9000 rpm for 15 minutes each with ultrapure water to remove unreacted species and afterwards freeze–dried overnight at -50°C under vacuum (3 mbar). Differently, sample d was purified with 3 additional washing cycles.

2.3. Characterization Techniques

The pH of the solutions/suspensions was measured by a Crison 5208 pH probe connected to a Crison GLP21 pH–meter (Crison Instruments S.A., Spain). Solid samples were characterized by X–ray powder diffraction (XRD), Variable pressure scanning electron microscopy (VPSEM), Fourier transform infrared spectroscopy (FTIR) and Raman microspectroscopy. Europium was quantified by inductively coupled plasma optical emission spectrometry (ICP–OES). Collagen, citrate, carbonate and the residual inorganic components were quantified by thermogravimetric analysis (TGA).

The XRD data were collected using a Bruker D8 Advance Vario diffractometer (Bruker GmbH, Karlsruhe, Germany) with a flat plate transmission geometry and $\text{Cu K}\alpha 1$ radiation (1.5406 \AA). Mineralized fibrils were deposited on Mylar films and supported on poly–methyl methacrylate (PMMA) sample holder for measurements. For low angle measurements a special circular slit, avoiding the direct beam and allowing the achievement of a perfect plain background from $2\theta 4.5^\circ$ to $8\text{--}9^\circ$, were constructed. VPSEM observations were performed with a Zeiss SUPRA40VP instrument (Carl Zeiss, Jena, Germany). Few mineralized fibrils were selected from each experiment and deposited/attached on conventional supports; then they were carbon–sputtered prior the observation.

FTIR spectroscopy analyses were recorded in transmission mode using a Perkin–Elmer Spectrum One FTIR spectrometer (Perkin–Elmer, Beaconsfield, UK) using the KBr pellet method. The pellets were prepared by mixing 1 mg of sample with $\sim 100 \text{ mg}$ of anhydrous KBr and then pressed with a hydraulic pump at 10 t into 7 mm diameter discs. Pure KBr pellets were used to record the background. FTIR spectra were recorded in transmittance mode within the wavenumber range from 4000 cm^{-1} to 400 cm^{-1} . Raman spectra were collected with a LabRAMHR spectrometer with backscattering geometry (Jobin–Yvon, Horiba, Japan). The excitation line was provided by a diode laser emitting at a

wavelength of 532 nm and a Peltier cooled charge–couple device (CCD) (1064 × 256 pixels) was used as detector. Spectrometer resolution was higher than 3 cm^{-1} . For each acquisition and depending on the quality of the spectra, signal average of two or three spectra and acquisition time between 100 and 500 s was performed. Some spectra were linearly base–line corrected.

The quantification of Eu was carried out by ICP–OES (Liberty 200, Varian, Palo Alto, CA, USA) employing a wavelength of 420.504 nm. Solid samples were dissolved in a diluted HNO_3 solution (~1 wt %) prior to the analysis. TGA analyses were performed using a STA 449F3 Jupiter (Netzsch GmbH, Selb, Germany) apparatus. About 10 mg of selected fibers in the sample were weighted in an alumina crucible and heated from room temperature to $1100 \text{ }^\circ\text{C}$ under air flow with a heating rate of $10 \text{ }^\circ\text{C}/\text{min}$. The weight losses were attributed to (i) adsorbed and structural water for the temperature range from room temperature to $220 \text{ }^\circ\text{C}$, (ii) collagen for the temperature range $220\text{--}600 \text{ }^\circ\text{C}$, (iii) citrate for the temperature range $600\text{--}760 \text{ }^\circ\text{C}$, (iv) carbonate ions for the temperature range $760\text{--}1000 \text{ }^\circ\text{C}$. The inorganic component was measured as residual at $1100 \text{ }^\circ\text{C}$ (See Figure S1, Supporting Information).

2.4. Luminescence Spectroscopy

Excitation and emission spectra of the mineralized fibrils prepared in presence of Eu^{3+} were recorded using a Cary Eclipse Varian Fluorescence Spectrophotometer (Varian Australia, Mulgrave, Australia). A front surface accessory was used to obtain the luminescence spectra, the luminescence lifetime (τ) and the relative luminescence intensities (R.L.I.) of the fibrils mineralized in presence of Eu^{3+} . The instrumental parameters for the characterization of samples in solid state were: $\lambda_{\text{exc}} = 240 \text{ nm}$, $\lambda_{\text{em}} = 614 \text{ nm}$, slit–width $_{\text{exc/em}} = 10/10 \text{ nm}$, the delay time (t_d) = $0.120 \text{ } \mu\text{s}$ and gate time (t_g) = 5 ms . Spectra were recorded with a photomultiplier voltage of 600 V . The excitation and emission spectra were recorded within the wavelength range $200\text{--}450 \text{ nm}$ and $450\text{--}750 \text{ nm}$, respectively. The luminescent spectrum of the sample $\text{Cit}_{\text{high}}\text{Eu}\text{--Col}/\text{Ap}$ was compared to those of citrate–coated Eu^{3+} –doped carbonated apatite nanoparticles ($13.3 \pm 2.6 \text{ wt } \% \text{ Eu}$) obtained in a previous work [26] and citrate–coated Ca^{2+} –doped $\text{EuPO}_4 \cdot \text{H}_2\text{O}$ ($43.7 \pm 0.3 \text{ wt } \% \text{ Eu}$, $4.9 \pm 0.1 \text{ wt } \% \text{ Ca}$) nanoparticles prepared recently in our laboratory.

2.5. Cytocompatibility Tests

GTL–16 (a human gastric carcinoma cell line) [31], MG–63 (a human osteosarcoma cell line; ATCC®CRL–1427™) and m17.ASC (a spontaneously immortalized mouse mesenchymal stem cell clone from subcutaneous adipose tissue) [32] cells were maintained in Dulbecco's modified Eagle's medium (DMEM, Sigma), supplemented with 10% FCS, 50 U/mL penicillin, and $50 \text{ } \mu\text{g}/\text{ml}$ streptomycin. For the assay, cells (12,000, 6,000 and 5,000 cells/well in 96–well plates, respectively) were incubated for 24 hours and then concentrations ranging from 0.1 to $100 \text{ } \mu\text{g}/\text{ml}$ of the different mineralized type I collagen fibrils were added in $100 \text{ } \mu\text{L}$ of fresh medium (DMEM, 10% fetal calf serum, antibiotics). After 72 hours incubation, cell viability was evaluated by the 3–(4,5–Dimethylthiazol–2–yl)–2,5–diphenyltetrazolium bromide) (MTT, Sigma.) colorimetric assay. Briefly, $20 \text{ } \mu\text{L}$ of MTT solution ($5 \text{ mg}/\text{ml}$ in a phosphate buffered saline PBS solution) were added to each well. The plate was then incubated at $37 \text{ }^\circ\text{C}$ for 3 hours. After the removal of the solution, $125 \text{ } \mu\text{L}$ of isopropanol, 0.2 M HCl were added to dissolve formazan crystals. $100 \text{ } \mu\text{L}$ were then removed carefully and the optical density was measured in a multiwell reader (2030 Multilabel Reader Victor TM X4, Perkin Elmer, Monza, Italy) at 570 nm . Viability of parallel cultures of untreated cells was taken as 100% viability, and values obtained from cells undergoing the different treatments were referred to this value. Cells were also incubated with Doxorubicin ($10 \text{ } \mu\text{g}/\text{ml}$) to promote cytotoxicity. Experiments were performed 3 times using 3 replicates for each sample.

3. Results and Discussion

3.1. Morphological, Chemical and Crystallographic Characteristics

In all experiments the obtained samples were composed of mineralized collagen fibrils and small amounts of inorganic precipitate. Figure 1 shows the VPSEM micrographs of mineralized fibrils obtained in the reference experiment (a), and in presence of citrate (b–d), citrate and Eu^{3+} (e) and only Eu^{3+} (f).

The diameter of the single fibrils was not significantly affected by citrate or by Eu^{3+} and it remained of about 200 nm. Most of the fibrils were fully mineralized and their coatings were formed by rounded shaped nanoparticles of 50–100 nm in diameter. The morphology of the mineral phase did not change among the different samples. The quantitative analysis reveals the successful incorporation of Eu^{3+} , in both samples prepared with and without the presence of citrate, but the highest amount of Eu^{3+} (2.4 wt %) was obtained in the sample $\text{Eu}/\text{Col}/\text{Ap}$ (Table 1). When citrate was added to the titrant solutions the percentage of inorganic residues measured by TGA decreased to 30–40 wt % in comparison to Col/Ap , while no significant effect was revealed when only Eu^{3+} was added. This result clearly shows the inhibitor effect of citrate in calcium phosphate precipitation. The composition of sample d was slightly different from that of the sample a, with a small decreasing amount of inorganic residues. This can be due to the fact that the deposited apatite was partially removed during the treatment with citrate.

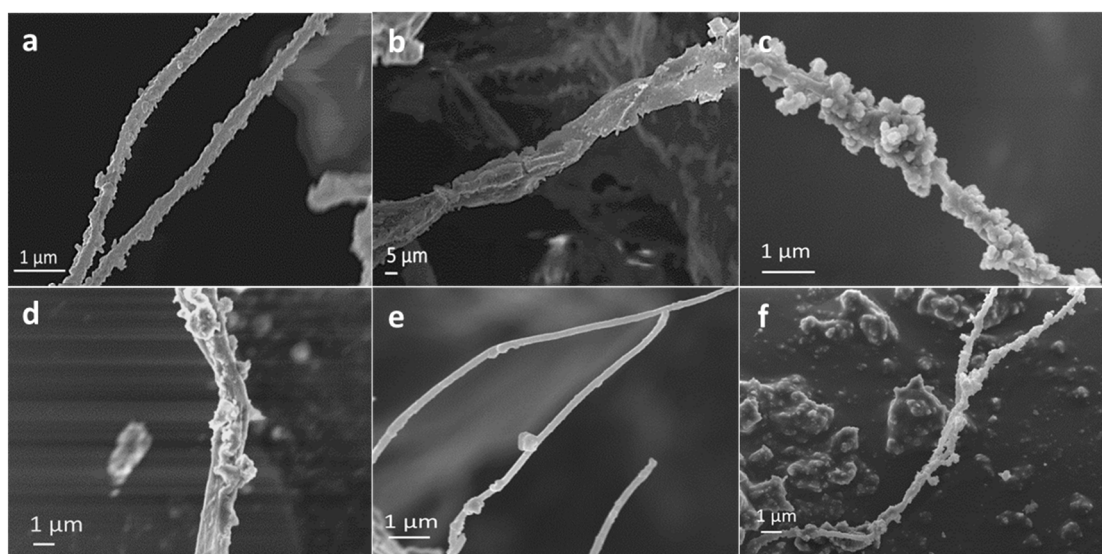


Figure 1. VPSEM micrographs of some selected mineralized fibrils of Table 1: (a) Col/Ap , (b) $\text{cit}_{\text{high}}\text{-Col}/\text{Ap}$, (c) $\text{cit}_{\text{low}}\text{-Col}/\text{Ap}$, (d) $\text{Col}/\text{Ap-cit}_{\text{high}}$, (e) $\text{cit}_{\text{high}}\text{-Eu}/\text{Col}/\text{Ap}$, and (f) $\text{Eu}/\text{Col}/\text{Ap}$.

The XRD patterns of mineralized collagen fibrils of the blank sample (a) as well as of samples prepared in presence of citrate (b,c,d), citrate and Eu^{3+} (e), and only Eu^{3+} (f), are reported in Figure 2A. The samples were attached on a Mylar film and supported on a PMMA sample holder; therefore the main reflections of the PMMA, that are located at $2\theta \sim 14.2^\circ$, 16.2° and $\sim 43^\circ$, are present. No reflections from the Mylar film were observed. Except for the signals of the support, the diffractograms of the mineralized collagen fibrils prepared in presence of citrate (b,c,d) did not show any remarkable diffraction peak; only very small reflections emerging from the bulging baseline in the 2θ range from $30^\circ\text{--}32^\circ$ were recorded indicating that the mineral component is mainly amorphous. The diffractograms of these latter samples showed a small peak at $\sim 29.5^\circ$ which can be attributed to a low amount of CaCO_3 (calcite, powder diffraction file PDF 00-005-0586) precipitated in the $\text{Ca}(\text{OH})_2$ suspension in contact with CO_2 (coming from the air) prior the titration. Differently, samples d ($\text{Col}/\text{Ap-cit}_{\text{high}}$) and f ($\text{Eu}/\text{Col}/\text{Ap}$) showed the distinguishing reflections of the apatite phase (PDF

01–071–5048), namely, the peaks at $2\theta = 25.87^\circ$ corresponding to the (002) plane, the broad reflection between 31° and 33° corresponding to planes (211), (112) and (300), the reflections at 33.9° and 39.8° attributed to the planes (202) and (310), and other minor peaks in the 2θ range from 40° – 55° [26]. These diffractograms are very similar to that of the reference sample a, demonstrating that in absence of citrate the obtained mineral phase is crystalline apatite. In addition, in Figure 2B the low angle measurements are reported revealing that no signals were present in the 2θ range from 4.5° to 9° , which excluded the presence of the octacalcium phosphate (OCP) phase in all the samples [33,34].

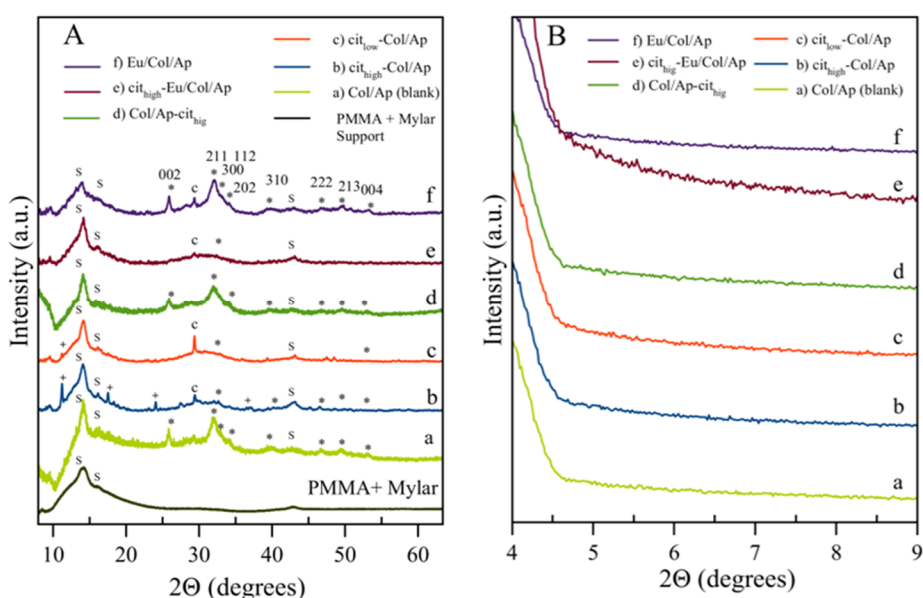


Figure 2. (A) X-ray diffraction patterns of mineralized type I collagen fibrils: a) Col/Ap, b) cit_{high} -Col/Ap, c) cit_{low} -Col/Ap, d) Col/Ap- cit_{high} , e) cit_{high} -Eu/Col/Ap, and f) Eu/Col/Ap. The XRD pattern of the PMMA sample holder, whose characteristic reflections are denoted with S, is plotted at the bottom of the graph. (*) denotes the signals of the apatite phase, (c) denotes the signals of calcite and (+) denotes the signals of sodium citrate dihydrate residues. (B) Low angle XRD measurements of the samples a–f.

It is worth to mention that sample d (Col/Ap- Cit_{high}) was submitted to 6 cycles of washing by centrifugation prior the XRD characterization. The objective was to extensively remove the citrate salts residues that can precipitate when a high concentration of citrate is employed namely sodium citrate dihydrate ($\text{C}_6\text{H}_5\text{Na}_3\text{O}_7 \cdot 2\text{H}_2\text{O}$; PDF 00–016–1170), sodium citrate pentahydrate ($\text{C}_6\text{H}_5\text{Na}_3\text{O}_7 \cdot 5\text{H}_2\text{O}$; PDF 00–016–0962), and calcium dicitrate tetrahydrate ($\text{Ca}_3(\text{C}_6\text{H}_5\text{O}_7)_2 \cdot 4\text{H}_2\text{O}$; PDF 00–028–2003). In fact, as mainly demonstrated in the XRD pattern of sample b, which was also synthesized in presence of the highest amount of citrate and purified only with 3 washing cycles, small amounts of citrate salts were present. The co-precipitation of some citrate salts residues with the apatite phase in Ca/citrate/phosphate solutions was also reported in previous works [35,36].

Table 1. Codes, details of the basic titrant solutions and composition of mineralized collagen.

Sample Identificación	Basic Titrant Solution	Mineral Phase	pHs (Initial; Final)	Eu (wt %)	Collagen (wt %)	Citrate (wt %)	Inorganic Residues (wt %)	Carbo-nate (wt %)
a. Col/Ap	0.495 M Ca(OH) ₂	Ap	12.5; 7.3	0	7.6 ± 0.8	0	83.5 ± 8.0	3.1 ± 0.3
b. cit _{high} -Col/Ap	0.495 M Ca(OH) ₂ + +0.990 M Na ₃ cit	ACP	13.5; 7.3	0	23.8 ± 2.0	5.3 ± 0.5	50.7 ± 5.0	8.5 ± 0.9
c. cit _{low} -Col/Ap	0.495 M Ca(OH) ₂ + 0.495 M Na ₃ cit	ACP	13.6; 7.1	0	34.7 ± 3.0	1.7 ± 0.2	59.3 ± 6.0	1.5 ± 0.2
d. Col/Ap-cit _{high}	0.495 M Ca(OH) ₂ + +0.990 M Na ₃ cit*	Ap	12.5; 9.8	0	13.8 ± 2.0	0.7 ± 0.1	76.6 ± 8.0	3.9 ± 0.4
e. cit _{high} -Eu/Col/Ap	0.495 M Ca(OH) ₂ + +0.990 M Na ₃ cit+ +0.010 M EuCl ₃	ACP	13.4; 7.2	0.6 ± 0.3	21.6 ± 2.0	5.9 ± 0.6	51.3 ± 5.0	8.1 ± 0.8
f. Eu/Col/Ap	0.495 M Ca(OH) ₂ + +0.010 M EuCl ₃	Ap	13.03; 7.3	2.4 ± 0.2	7.5 ± 0.8	0	79.5 ± 8.0	1.6 ± 0.2

Acidic collagen solutions were prepared by dissolving 500 mg of type I collagen in 10 mL of ~0.295 M H₃PO₄ (pH = 1.30); a) Col/Ap, b) cit_{high}-Col/Ap, c) cit_{low}-Col/Ap, d) Col/Ap-cit_{high}, e) cit_{high}-Eu/Col/Ap, and f) Eu/Col/ *0.99 M Na₃cit solution was added at the end of the neutralization reaction. The mineral phase, Ap (apatite) or ACP (amorphous calcium phosphate) was identified by XRD. The amounts of collagen (wt %), citrate (wt %) and carbonate (wt %) were determined by TGA.

3.2. FTIR and Raman Spectral Features

Additional characterizations were carried out analyzing the samples by FTIR and Raman microspectroscopy. The principal FTIR absorption bands of type I collagen fibrils assembled in 0.29 M H_3PO_4 are shown as reference in Figure 3A. This spectrum revealed the typical bands of amide B ($\sim 3065\text{ cm}^{-1}$, stretching C–H), I ($\sim 1658\text{ cm}^{-1}$, stretching C=O), II (1535 cm^{-1} , stretching C–N), and III ($\sim 1236\text{ cm}^{-1}$, C–N stretching and bending N–H) [37] which are associated with the triple helical conformation of type I collagen fibrils. The FTIR spectrum of this sample also exhibit bands at 1035 and 1080 cm^{-1} , which arise from the C–O stretching and C–O–C stretching absorption modes of the carbohydrate moieties [38], a band at 2920 cm^{-1} which corresponds to C–H anti-symmetrical stretching, and a band at 1453 cm^{-1} which corresponds to the C=H stretching [36]. Additionally, two bands at 498 and 592 cm^{-1} are attributed to phosphate groups.

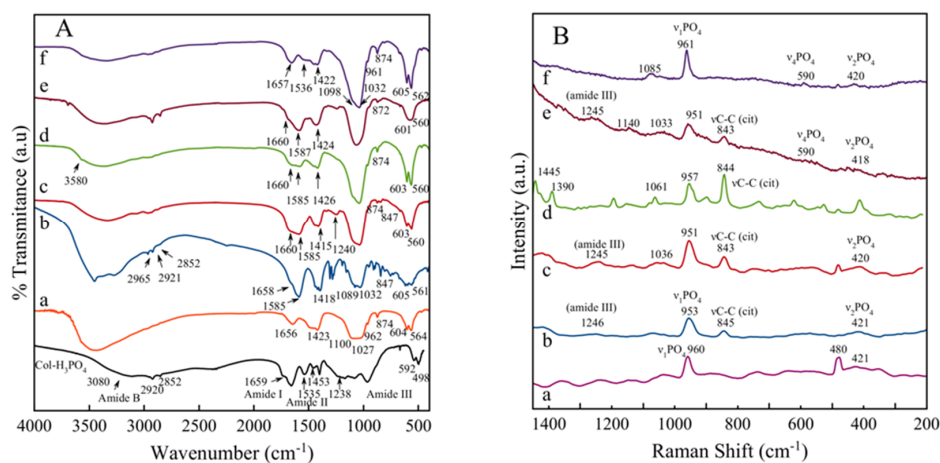


Figure 3. (A) FTIR spectra of mineralized type I collagen fibrils: a) Col/Ap, b) cit_{high}-Col/Ap, c) cit_{low}-Col/Ap, d) Col/Ap-cit_{high}, e) cit_{high}-Eu/Col/Ap, and f) Eu/Col/Ap. The FTIR spectrum of type I collagen fibrils assembled in 0.295 M H_3PO_4 is plotted at the bottom of the graph. (B) Raman spectra of mineralized type I collagen fibrils: samples a–f. The band at $\sim 480\text{ cm}^{-1}$ belongs to Si–O of the glass support.

Figure 3A shows the FTIR spectra of the different mineralized fibrils. Some of the typical absorption bands of collagen such as the amides I, II and the less intense amide III were observed at around 1657 – 1660 , 1535 and 1240 cm^{-1} , respectively. In some spectra the amides A and B are overlapped with the H_2O band between 3600 cm^{-1} and 2600 cm^{-1} . The presence of apatitic –OH stretching at around 3580 cm^{-1} in the samples containing apatite was not clearly detected, due to the presence of CO_3^{2-} ions replacing partially the –OH, as well as their poor hydroxylation, as customary for the bio-inspired apatites. Only in the sample Col/Ap-cit_{high} this peak appeared but its intensity is very small. In the region 400 – 1800 cm^{-1} the typical spectral features of apatitic compounds can be revealed; the main band at 1000 – 1100 cm^{-1} corresponds to the asymmetric stretching mode of PO_4^{3-} groups ($\nu_3\text{PO}_4$) and the shoulder at $\sim 961\text{ cm}^{-1}$ is ascribed to the symmetric stretching of PO_4^{3-} ($\nu_1\text{PO}_4$) while the less intense bands at ~ 603 and 560 cm^{-1} are due to the bending mode of PO_4^{3-} groups ($\nu_4\text{PO}_4$). A shoulder at $\sim 532\text{ cm}^{-1}$ in the $\nu_4\text{PO}_4$ domain can be assigned to non-apatitic (surface) HPO_4^{2-} ions and it is only visible on the sample Eu–Col/Ap obtained in absence of citrate [26]. The bands of carbonate ions were also visible, namely the signals of the $\nu_3\text{CO}_3$ mode at around $\sim 1415\text{ cm}^{-1}$, partially overlapped with carboxylate COO– citrate bands as the one located at 1466 cm^{-1} [39], and the bulging peak at around 874 cm^{-1} of the $\nu_2\text{CO}_3$ mode. Besides the apatitic vibrational contributions, a band at ~ 1585 – 1587 cm^{-1} was also noticed in all samples prepared in presence of citrate ions, which was ascribed to the antisymmetric stretching frequencies of the carboxylate groups of the citrate. This band is wide and it probably overlaps with the amide II band of collagen. This band is sharper in samples

prepared with the high concentration of citrate. Bands at $\sim 2920\text{ cm}^{-1}$ and $\sim 847\text{ cm}^{-1}$ were assigned to νCH_2 and δCOO modes [40] of the citrate ions, respectively. Figure 3B shows the complementary characterization of the spectral features of mineralized fibrils by Raman microspectroscopy. Overall, the amide I band (stretching C=O) is centered at 1668 cm^{-1} and the amide III ($\sim 1236\text{ cm}^{-1}$, C–N stretching and bending N–H) at $1246\text{--}1248\text{ cm}^{-1}$ [41]. The spectral features of apatite arise at $957\text{--}961\text{ cm}^{-1}$ ($\nu_1\text{ PO}_4$), $418\text{--}420\text{ cm}^{-1}$ ($\nu_2\text{ PO}_4$), 590 cm^{-1} ($\nu_4\text{ PO}_4$), and those of citrate at around $1445\text{--}1450\text{ cm}^{-1}$ and $843\text{--}845\text{ cm}^{-1}$ ($\nu\text{ C--C}$) [26]. This latter band was not observed in the spectra of samples Col/Ap and Eu–Col/Ap prepared in absence of citrate. It was observed that in all the Raman spectra of the samples prepared using citrate ions in the titrant solutions, the $\nu_1\text{ PO}_4$ bands appeared at $951\text{--}953\text{ cm}^{-1}$ indicating the presence of ACP [42] in agreement with the XRD data. In addition it was also observed that the intensity ratio between the peak at $958\text{--}959\text{ cm}^{-1}$ ($\nu_1\text{ PO}_4$) and that centered at $843\text{--}845\text{ cm}^{-1}$ ($\nu\text{ C--C}$ of citrate) is higher when the lowest amount of citrate was used, which confirm that citrate slowed down the growth of apatite and thus behaved as an inhibitor.

In this work mineralized type I collagen fibrils were prepared, trying to recreate the basic building block of human mineralized tissue, as well as to develop a new bioinspired nanostructured material in which the collagen fibrils are mineralized with Eu^{3+} -doped apatite nanocrystals. The results revealed by that adding citrate to the titrant $\text{Ca}(\text{OH})_2$ solution, the mineralized fibrils are basically constituted of amorphous calcium phosphate (ACP) or incipiently formed poorly crystalline apatite nanoparticles. Differently, the experiments carried out either adding citrate after the neutralization reaction or in absence of citrate yielded mineralized fibrils constituted of apatite nanocrystals.

When the citrate was added in the titrant $\text{Ca}(\text{OH})_2$ solution with a Cit/Ca molar ratio equal to 2 or 1, it acted as an inhibitor of the transformation from ACP to nanocrystalline apatite, slowing down this process and enhancing the long term stability of ACP, similarly to as previously found by Delgado–López et al. [17]. Differently, when citrate was added at the end of the neutralization reaction, the mineral phase was mainly apatite, suggesting that the ACP to apatite transformation occurred during the titration process. According to the data reported by Delgado–López et al [17] the effect of citrate to inhibit the precipitation of the mineral phase is a concentration-dependent phenomenon that should be driven by the adsorption of citrate on the ACP surface. As the syntheses were carried out by titrating a strong acid solution with a strong base, the pH of the solution will progressively increase to neutrality (pHs 7.0–7.3) at the endpoint of the neutralization reaction. In these conditions the three $-\text{COOH}$ groups of the citrate are fully deprotonated according to their pKs ($\text{pK}_1 = 3.13$, $\text{pK}_2 = 4.76$, $\text{pK}_3 = 6.40$ [43]), though only one or two can electrostatically interact with the positively charged surface $\langle\text{Ca}^{\delta+}$ of the ACP [44]. Adding an excess of titrant solution may yield the precipitation of sodium citrate salts. This was the case of sample b (Cit_{high}–Col/Ap) in which some residues of citrate salts were found.

3.3. Luminescent Properties of Eu^{3+} -Doped Mineralized Collagen Fibrils

The main aim of this work was not the study of basic mechanisms of collagen mineralization and the effect of citrate in this process, which was already reported [17,18], but the preparation for the first time of a new luminescent bioinspired composite Col/Ap material. Therefore the luminescent properties of the as-synthesised samples were fully investigated. Figure 4 shows the luminescence properties of Eu^{3+} -doped mineralized collagen fibrils in solid state. The luminescence emission (sensitized fluorescence) is due to the formation of highly fluorescent complexes between Eu^{3+} and the phosphate ions within the Eu^{3+} -doped calcium phosphate nanoparticles [26].

The sensitized fluorescence results from the ligand absorbing light, the energy of which is then transferred to Eu^{3+} which emits the energy as narrow-banded, line-type fluorescence with a long Stokes shift (over 250 nm) and an exceptionally long fluorescence decay time (up to 1 ms) [45].

The observed excitation wavelengths were 240, 321, 364, 385 and 395 nm. The broad band between 200 and 300 nm, centered at 240 nm, corresponds to charge transfer (called charge transfer band; CTB), which occurs by electron delocalization from the filled 2p shell of O^{2-} to the partially filled 4f shell of Eu^{3+} . Also, this band can partly be attributed to the charge transfer transition $\text{X}^{5+}\text{--O}^{2-}$ [46,47]. The

weaker bands centered at 321, 364, 385 and 395 nm correspond to the excitation of the Eu^{3+} ; ${}^7\text{F}_0 \rightarrow {}^5\text{H}_6$, ${}^7\text{F}_0 \rightarrow {}^5\text{D}_4$, ${}^7\text{F}_0 \rightarrow {}^5\text{L}_7$ and ${}^7\text{F}_0 \rightarrow {}^5\text{L}_6$ transitions [48].

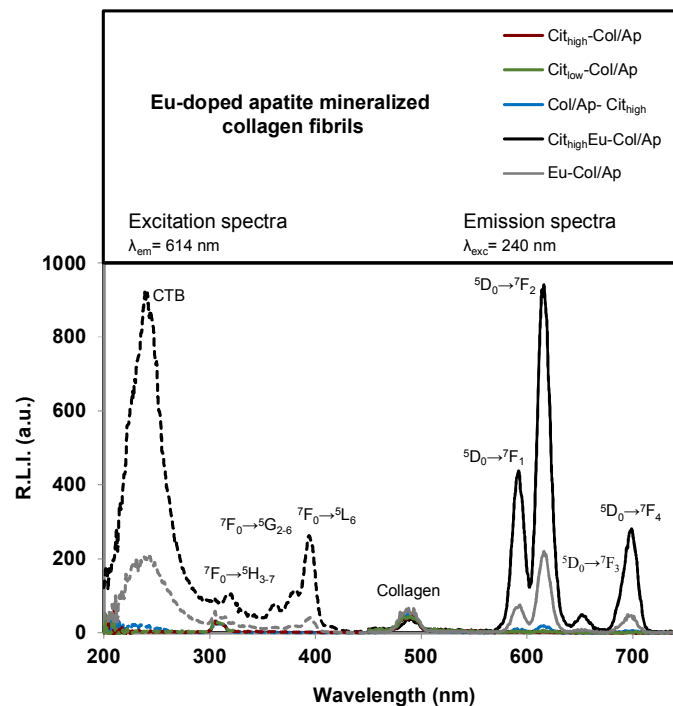


Figure 4. Uncorrected excitation (dashed lines) and emission (solid lines) spectra of different Eu^{3+} -doped apatite mineralized collagen fibrils. Slit-width_{exc/em} = 10/10 nm, t_d = 120 μs , t_g = 5 ms and voltage detector = 600 v.

The emission spectra show an emission band centered at 490 nm which is not affected by the concentration of $\text{Eu}(\text{III})$ and therefore is shown in all the materials. This luminescence emission can be attributed to the collagen, more precisely to proline aminoacids [49,50]. On the other hand, there are several narrow bands centered at 592, 614, 650 and 699 nm which correspond to the Eu^{3+} ${}^5\text{D}_0 \rightarrow {}^7\text{F}_1$, ${}^5\text{D}_0 \rightarrow {}^7\text{F}_2$, ${}^5\text{D}_0 \rightarrow {}^7\text{F}_3$ and ${}^5\text{D}_0 \rightarrow {}^7\text{F}_4$ transitions, respectively [48].

As can be observed, the maximum luminescence emission is obtained when excitation and emission wavelengths are 240 and 614 nm, respectively. The excitation wavelength of 240 nm corresponds to the CTB band and the emission wavelength of 614 nm corresponds to the hypersensitive transition without inversion center (${}^5\text{D}_0 \rightarrow {}^7\text{F}_2$) which results in the highest relative luminescence intensity (R.L.I) when nanosized particles dominates the luminescence emission [51]. Only the two materials doped with Eu^{3+} ($\text{Cit}_{\text{high}}\text{Eu-Col/Ap}$ and Eu-Col/Ap) show a strong luminescent emission at these wavelengths.

On the other hand, $\text{Cit}_{\text{high}}\text{Eu-Col/Ap}$ shows higher luminescence intensity than Eu-Col/Ap , even if the Eu^{3+} doping is a fourth of the latter. The only difference in the preparation of both materials is the presence of citrate in the titrant solution. Therefore, the adsorbed citrate affects the luminescence properties of the material. It can be due to several reasons: 1) the presence of citrate adsorbed on the surface of the nanoparticle which increases the luminescence of the Eu^{3+} ; 2) because citrate affects the amorphous or crystalline nature of the calcium phosphate, in fact $\text{Cit}_{\text{high}}\text{Eu-Col/Ap}$ is amorphous and Eu-Col/Ap is crystalline; 3) a combination of both causes.

The luminescent emission of $\text{Cit}_{\text{high}}\text{Eu-Col/Ap}$ is very intense and it can be seen by naked eye. Figure 5 shows a picture of $\text{Cit}_{\text{high}}\text{Eu-Col/Ap}$ (left) and $\text{Cit}_{\text{high}}\text{-Col/Ap}$ (right) materials under sunlight and UV-light (324 nm) illuminations. Under sunlight (Figure 5, down) both materials shows a white color. Under UV illumination (Figure 5, up) $\text{Cit}_{\text{high}}\text{-Col/Ap}$ shows a blue color while $\text{Cit}_{\text{high}}\text{Eu-Col/Ap}$ is purple. It is due to the fluorescence emission of both materials; $\text{Cit}_{\text{high}}\text{-Col/Ap}$

shows the blue fluorescence emission of the collagen (490 nm) and $\text{Cit}_{\text{high}}\text{Eu-Col/Ap}$ shows the same blue emission as well as the red emission (614 nm) of the Eu^{3+} , resulting in a purple color. It has to bear in mind that this picture shows fluorescence emission ($t_d = 0\mu\text{s}$) while Figure 4 shows sensitized fluorescence ($t_d = 120\mu\text{s}$) and for this reason the intensity of the blue emission of the collagen in Figure 4 is very low. However, it can be seen by naked eyes in this picture.

Figure 6 compares the luminescent properties of $\text{Cit}_{\text{high}}\text{Eu-Col/Ap}$ with those of citrate-coated Eu^{3+} -doped carbonated apatite nanoparticles ($13.3 \pm 2.6\text{ wt \% Eu}$) obtained in a previous work [26] and citrate-coated Ca^{2+} -doped $\text{EuPO}_4\cdot\text{H}_2\text{O}$ ($43.7 \pm 0.3\text{ wt \% Eu}$, $4.9 \pm 0.1\text{ wt \% Ca}$) nanoparticles prepared recently in our laboratory. It is possible to conclude that the luminescence properties of all of them are practically the same, varying only in the emission at 490 nm because the particles did not contain collagen. The R.L.I. cannot be compared because the spectra were recorded with different instrumental conditions due to the differences in the luminescence quantum yields.

An important parameter in sensitized luminescent complexes is the luminescence lifetime (τ); see Figure 7. For each sample, the decay profile was analyzed as a single exponential component ($\text{RLI} = A \cdot e^{-t/\tau} + C$) [52].

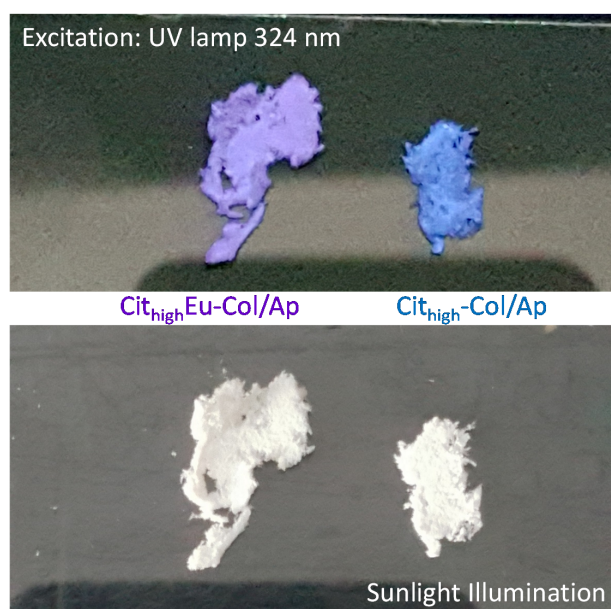


Figure 5. Picture of $\text{Cit}_{\text{high}}\text{Eu-Col/Ap}$ (left) and $\text{Cit}_{\text{high}}\text{-Col/Ap}$ (right) under sunlight (down) and 324 nm UV-lamp illumination (up).

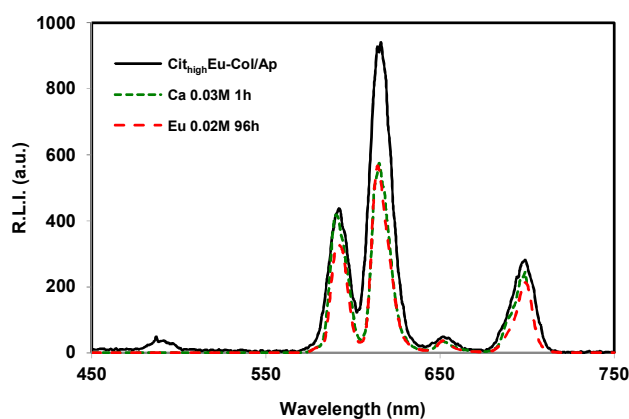


Figure 6. Uncorrected emission spectra of $\text{Cit}_{\text{high}}\text{Eu-Col/Ap}$ (solid black line), citrate-coated Eu^{3+} -doped carbonated apatite nanoparticles ($13.3 \pm 2.6\text{ wt \% Eu}$) (dotted green line) and citrate-coated Ca^{2+} -doped $\text{EuPO}_4\cdot\text{H}_2\text{O}$ ($43.7 \pm 0.3\text{ wt \% Eu}$, $4.9 \pm 0.1\text{ wt \% Ca}$) nanoparticles (dashed red line).

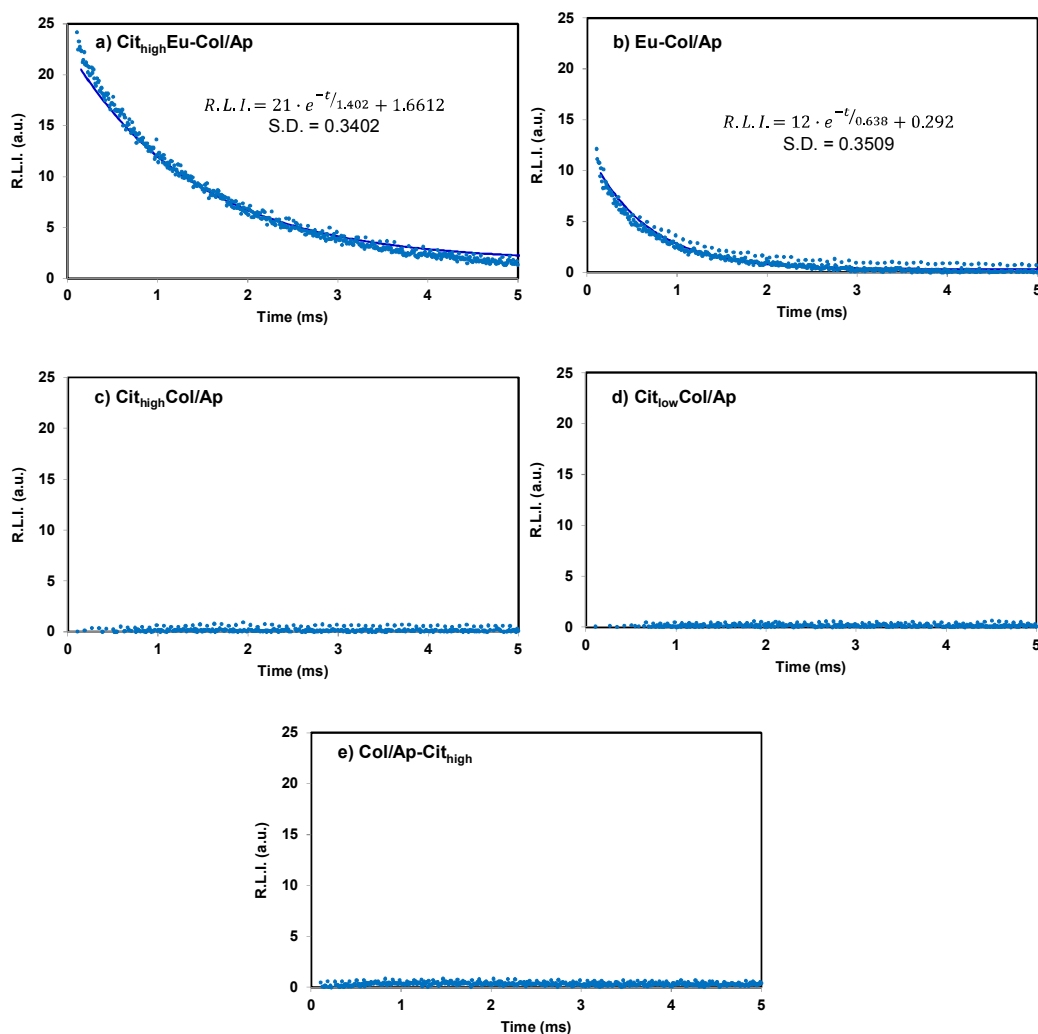


Figure 7. Luminescence decay curve of the different Eu-doped apatite mineralized collagen fibrils, i.e. (a) cit_{high}-Col/Ap, (b) Eu-Col/Ap, (c) cit_{high}-Col/Ap, (d) cit_{low}-Col/Ap, and (e) Col/Ap-cit_{high} $\lambda_{exc/em} = 240/614$ nm, slit-widths_{exc/em} = 10/0 nm, and detector voltage = 600 V. Circles correspond to experimental data and lines to the fitting equation.

The decay curves of the free Eu³⁺ samples are practically flat indicating that no sensitized luminescence is recorded; this is due to the fact that they do not contain Eu³⁺ in their structure. In addition, the highest lifetime is shown by Cit_{high}Eu-Col/Ap (1402 μ s) while the lifetime of Eu-Col/Ap is practically half of it (638 μ s). It can be due to the same reasons why the presence of citrate increases the luminescence intensity: 1) because the citrate itself stabilized the excited state of the Eu³⁺ ions; 2) because the presence of citrate affects the amorphous or crystalline nature of the calcium phosphate, which influences over the deactivation of the excited states of the Eu³⁺; 3) both effects at the same time.

3.4. Cytocompatibility of the Mineralized Type I Collagen Fibrils

In view of a possible in vivo use of these composites, the cytocompatibility of the different samples of mineralized type I collagen fibrils was tested in a MTT assay on the GTL-16 human carcinoma cells, on MG-63 human osteosarcoma cells and on the m17.ASC murine mesenchymal stem cells, after incubation at concentrations ranging from 0.1 to 100 μ g/mL (Figure 8). Only the sample in which citrate was added just after the neutralization reaction (sample d, Col/Ap-cit_{high}) displayed some toxicity, in a dose-dependent manner, which was more detectable on the more sensitive MG-63 and m17.ASC cell lines (Figure 8 middle and down panels) and clearly evident also on GTL-16 cells at the highest concentration tested of 100 μ g/mL (Figure 8, up). In any case cell viability was always higher

than 70%, which is the cut-off indicated by ISO 10993-5:2009 [53]. The three cells lines were similarly sensitive to the toxic activity of Doxorubicin, which reduced their viability to less than 40%, when it was added at a 10 $\mu\text{g}/\text{mL}$ final concentration (data not shown). All together these data show a high cytocompatibility of the mineralized type I collagen fibrils, doped with Eu^{3+} and coated with citrate, and open new perspectives to possible in vivo applications, namely in the field of tissue engineering, regenerative medicine and bioimaging.

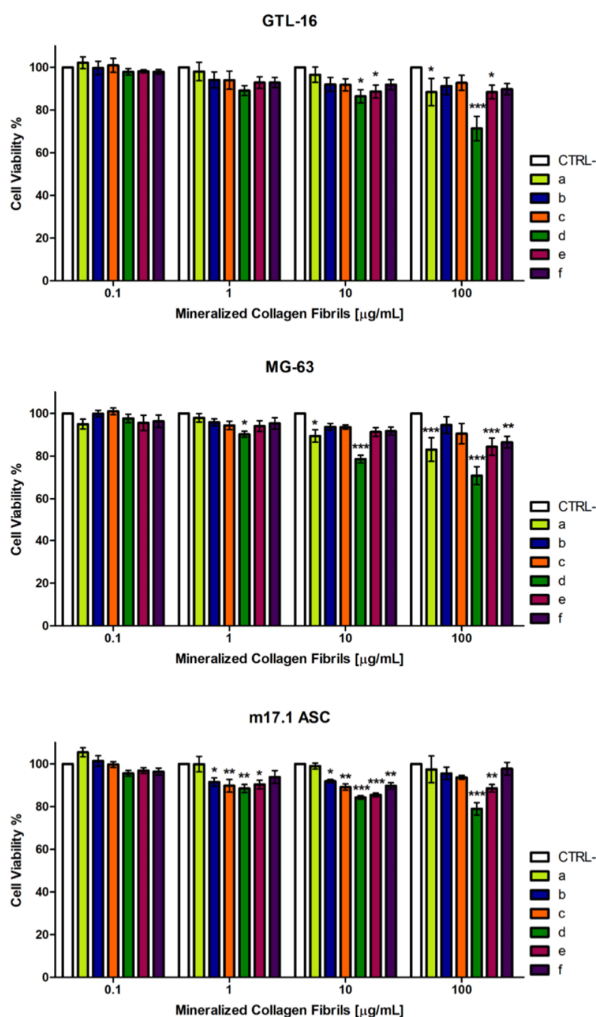


Figure 8. Cytocompatibility of the different Eu-doped and citrate-coated apatite mineralized collagen fibrils. GTL-16, MG-63 and m17.ASC cells were incubated with the different types of fibrils (a, Col/Ap; b, cit_{high}-Col/Ap; c, cit_{low}-Col/Ap; d, Col/Ap-cit_{high}; e, cit_{high}-Eu/Col/Ap; f, Eu/Col/Ap) for three days and their viability was assessed in MTT assays. Data represent means \pm sd of three independent experiments performed in triplicates and statistical analyses were carried on using One-way ANOVA, with Bonferroni comparison test. For statistical analysis all data were compared to untreated samples (* $p < 0.05$, ** $p < 0.01$, *** $p < 0.001$).

4. Conclusions

New nanostructured hybrid composites based on collagen and calcium phosphates have been synthesized in presence of citrate and Eu^{3+} . In absence of citrate the collagen fibrils were assembled and mineralized with nanocrystalline apatites. When citrate was added in the titrant solution in a Cit/Ca molar ratio 2 or 1, it acted as an inhibitor of the ACP to nanocrystalline apatite transformation, slowing down the transformation process and enhancing the long term stability of the amorphous particles associated to the collagen fibrils. The addition of Eu^{3+} and citrate in the titrant solutions resulted

mainly in the formation of Eu³⁺-doped citrate-coated ACP/collagen fibrils whose relative luminescent intensity (R.L.I.) and luminescence lifetime are superior to those of Eu-doped apatite/collagens prepared in absence of citrate. Although, dedicated *in vivo* tests are required to validate their biological performances, the as-synthesised bioinspired composites, thanks to their intrinsic bioactivity, cytocompatibility, bioresorbability and luminescent properties, could find in the future interesting applications in tissue engineering and bioimaging.

Supplementary Materials: The following is available online at <http://www.mdpi.com/2073-4352/9/1/13/s1>. Figure S1: a) TGA curves of mineralized collagen fibrils (Col/Ap blank sample) and b) Eu-doped citrate coated mineralized collagen fibrils (sample C_{high}Eu-Col/Ap).

Author Contributions: Conceptualization, Jaime Gómez Morales and Michele Iafisco; Investigation, Jaime Gómez Morales, Raquel Fernández Penas, Cristóbal Verdugo Escamilla, Lorenzo Degli Esposti, Michele Iafisco, Maria Prat, Francesca Oltolina and Jorge Fernando Fernández Sánchez; Methodology, Raquel Fernández Penas, Maria Prat, Francesca Oltolina, Jorge Fernando Fernández Sánchez; Supervision, Jaime Gómez Morales; Writing – original draft, Jaime Gómez Morales.

Funding: This research was funded by Spanish MINEICO and co-funded by FEDER (grant number MAT2014-60533-R). C. V.-E. acknowledges the Spanish MINEICO for his contract PTA2015-11103-I. M.I. acknowledges support by the Italian National Research Program–National Research Council (PNRCNR) Aging Program 2012–2014. The Excellence Network of Crystallography and Crystallization “Factoría de Cristalización” FIS2015-71928-REDC funded by Spanish MINEICO is also acknowledged.

Acknowledgments: The authors acknowledge the Centre of Scientific Instrumentation of the University of Granada for technical assistance in scanning electron microscopy.

Conflicts of Interest: The authors declare no conflict of interest. The funding sponsors had no role in the design of the study; in the collection, analyses, or interpretation of data; in the writing of the manuscript, and in the decision to publish the results.

References

1. Wegst, U.G.K.; Bai, H.; Saiz, E.; Tomsia, A.P.; Ritchie, R.O. Bioinspired structural materials. *Nat. Mat.* **2015**, *14*, 23–36. [[CrossRef](#)]
2. Lowenstam, H.A.; Weiner, S. *On Biomineralization*; Oxford University Press: Oxford, UK, 1989.
3. Mann, S. *Biomineralization: Principles and Concepts in Bioinorganic Materials Chemistry*; Oxford University Press: Oxford, UK, 2001; ISBN 9780198508823.
4. Weiner, S.; Wagner, H.D. The material bone: Structure–mechanical functions relations. *Ann. Rev. Mater. Sci.* **1998**, *28*, 271–298. [[CrossRef](#)]
5. Nudelman, F.; Pieterse, K.; George, A.; Bomans, P.H.; Friedrich, H.; Brylka, L.J.; Hilbers, P.A.; de With, G.; Sommerdijk, N.A. The role of collagen in bone apatite formation in the presence of hydroxyapatite nucleation inhibitors. *Nat. Mater.* **2010**, *9*, 1004–1009. [[CrossRef](#)]
6. Nudelman, F.; Lausch, A.J.; Sommerdijk, N.A.J.M.; Sone, E.D. *In vitro* models of collagen biomineralization. *J. Struct. Biol.* **2013**, *183*, 258–269. [[CrossRef](#)] [[PubMed](#)]
7. Shoulders, M.D.; Raines, R.T. Collagen structure and stability. *Ann. Rev. Biochem.* **2009**, *78*, 929–958. [[CrossRef](#)]
8. Orgel, J.P.; Miller, A.; Irving, T.C.; Fischetti, R.F.; Hammersley, A.P.; Wess, T.J. The *in situ* supermolecular structure of type I collagen. *Structure* **2001**, *9*, 1061–1069. [[CrossRef](#)]
9. Ishikawa, K. Bone Substitute Fabrication Based on Dissolution–Precipitation Reactions. *Materials* **2010**, *3*, 1138–1155. [[CrossRef](#)]
10. Gómez-Morales, J.; Iafisco, M.; Delgado-López, J.M.; Sarda, S.; Druet, C. Progress on the preparation of nanocrystalline apatites and surface characterization: Overview of fundamental and applied aspects. *Prog. Cryst. Growth Charact. Mater.* **2013**, *59*, 1–46. [[CrossRef](#)]
11. Hara, E.S.; Okada, M.; Nagaoka, N.; Hattori, T.; Kuboki, T.; Nakano, T.; Matsumoto, T. Bioinspired Mineralization Using Chondrocyte Membrane Nanofragments. *ACS Biomater. Sci. Eng.* **2018**, *4*, 617–625. [[CrossRef](#)]
12. Hu, Y.Y.; Rawal, A.; Schmidt-Rohr, K. Strongly bound citrate stabilizes the apatite nanocrystals in bone. *Proc. Natl. Acad. Sci. USA* **2010**, *107*, 22425–22429. [[CrossRef](#)]
13. Davies, E.; Müller, K.H.; Wong, W.C.; Pickard, C.J.; Reid, D.G.; Skepper, J.N.; Duer, M.J. Citrate bridges between mineral platelets in bone. *Proc. Natl. Acad. Sci. USA* **2014**, *111*, E1354–E1363. [[CrossRef](#)] [[PubMed](#)]

14. Delgado-López, J.M.; Frison, R.; Cervellino, A.; Gómez-Morales, J.; Guagliardi, A.; Masciocchi, N. Crystal Size, Morphology, and Growth Mechanism in Bio-Inspired Apatite Nanocrystals. *Adv. Funct. Mater.* **2014**, *24*, 1090–1099. [[CrossRef](#)]
15. Iafisco, M.; Ramírez-Rodríguez, G.B.; Sakhno, Y.; Tampieri, A.; Martra, G.; Gómez-Morales, J.; Delgado-López, J.M. The growth mechanism of apatite nanocrystals assisted by citrate: Relevance to bone biomineralization. *CrystEngComm* **2015**, *17*, 507–511. [[CrossRef](#)]
16. Costello, L.C.; Chellaiah, M.; Zou, J.; Franklin, R.B.; Reynolds, M.A. The status of citrate in the hydroxyapatite/collagen complex of bone; and its role in bone formation. *J. Regen. Med. Tissue Eng.* **2014**, *3*, 4. [[CrossRef](#)]
17. Delgado-López, J.M.; Bertolotti, F.; Lyngsø, J.; Pedersen, J.S.; Cervellino, A.; Masciocchi, N.; Guagliardi, A. The synergic role of collagen and citrate in stabilizing amorphous calcium phosphate precursors with platy morphology. *Acta Biomater.* **2017**, *49*, 555–562. [[CrossRef](#)] [[PubMed](#)]
18. Shao, C.; Zhao, R.; Jiang, S.; Yao, S.; Wu, Z.; Jin, B.; Yang, Y.; Pan, H.; Tang, R. Citrate Improves Collagen Mineralization via Interface Wetting: A Physicochemical Understanding of Biomineralization Control. *Adv. Mater.* **2018**, *30*, 1704876. [[CrossRef](#)] [[PubMed](#)]
19. Xie, B.; Nancollas, G.H. How to control the size and morphology of apatite nanocrystals in bone. *Proc. Natl. Acad. Sci. USA* **2010**, *107*, 22369–22370. [[CrossRef](#)]
20. Rodríguez-Ruiz, I.; Delgado-López, J.M.; Durán-Olivencia, M.A.; Iafisco, M.; Tampieri, A.; Colangelo, D.; Prat, M.; Gómez-Morales, J. pH-Responsive Delivery of Doxorubicin from Citrate-Apatite Nanocrystals with Tailored Carbonate Content. *Langmuir* **2013**, *29*, 8213–8221. [[CrossRef](#)]
21. Delgado-Lopez, J.M.; Iafisco, M.; Rodríguez-Ruiz, I.; Tampieri, A.; Prat, M.; Gómez-Morales, J. Crystallization of bioinspired citrate-functionalized nanoapatite with tailored carbonate content. *Acta Biomater.* **2012**, *8*, 3491–3499. [[CrossRef](#)]
22. Boccaccini, A.R.; Blaker, J.J. Bioactive composite materials for tissue engineering scaffolds. *Expert Rev. Med. Devices* **2005**, *2*, 303–317. [[CrossRef](#)]
23. Sprio, S.; Sandri, M.; Panseri, S.; Cunha, C.; Tampieri, A. Hybrid Scaffolds for Tissue Regeneration: Chemotaxis and Physical Confinement as Sources of Biomimesis. *J. Nanomater.* **2012**, 418281. [[CrossRef](#)]
24. Sprio, S.; Sandri, M.; Iafisco, M.; Panseri, S.; Adamaiano, A.; Comparodoni, E.; Tampieri, A. Bio-inspired assembling/mineralization process as a flexible approach to develop new smart scaffolds for the regeneration of complex anatomical regions. *J. Eur. Ceram. Soc.* **2016**, *36*, 2857–2867. [[CrossRef](#)]
25. Irizarry, A.R.; Yan, G.; Zeng, Q.; Lucchesi, J.; Hamang, M.J.; Ma, Y.L.; Rong, J.X. Defective enamel and bone development in sodium-dependent citrate transporter (NaCT) Slc13a5 deficient mice. *PLoS ONE* **2017**, *12*, e0175465. [[CrossRef](#)] [[PubMed](#)]
26. Gómez-Morales, J.; Verdugo-Escamilla, C.; Fernández-Penas, R.; Parra-Milla, C.M.; Drouet, C.; Maube-Bosc, F.; Oltolina, F.; Prat, M.; Fernández-Sánchez, J.F. Luminescent biomimetic citrate-coated europium doped carbonated apatite nanoparticles for use in bioimaging: Physico-chemistry and cytocompatibility. *RSC Adv.* **2018**, *8*, 2385–2397. [[CrossRef](#)]
27. Feng, W.; Wee Beng, T.; Yong, Z.; Xianping, F.; Minquan, W. Luminescent nanomaterials for biological labelling. *Nanotechnology* **2006**, *17*, R1–R13. [[CrossRef](#)]
28. Piccirillo, C.; Adamiano, A.; Tobaldi, D.M.; Montalti, V.; Manzi, J.; Lima Castro, P.M.; Panseri, S.; Montesi, M.; Sprio, S.; Tampieri, A.; et al. Luminescent calcium phosphate bioceramics doped with europium derived from fish industry byproducts. *J. Am. Ceram. Soc.* **2017**, *100*, 3402–3414. [[CrossRef](#)]
29. Tampieri, A.; Celotti, G.; Landi, E.; Sandri, M.; Roveri, N.; Falini, G. Biologically inspired synthesis of bone-like composite: Self-assembled collagen fibers/hydroxyapatite nanocrystals. *J. Biomed. Mater. Res. Part A* **2003**, *67*, 618–625. [[CrossRef](#)]
30. Tampieri, A.; Sandri, M.; Landi, E.; Pressato, D.; Francioli, S.; Quarto, R.; Martin, I. Design of graded biomimetic osteochondral composite scaffolds. *Biomaterials* **2008**, *29*, 3539–3546. [[CrossRef](#)]
31. Giordano, S.; Ponzetto, C.; Di Renzo, M.F.; Cooper, C.S.; Comoglio, P.M. Tyrosine kinase receptor indistinguishable from the c-met protein. *Nature* **1989**, *339*, 155–156. [[CrossRef](#)]
32. Zamperone, A.; Pietronave, S.; Merlin, S.; Colangelo, D.; Ranaldo, G.; Medico, E.; Di Scipio, F.; Berta, G.N.; Follenzi, A.; Prat, M. Isolation and characterization of a spontaneously immortalized multipotent mesenchymal cell line derived from mouse subcutaneous adipose tissue. *Stem Cells Dev.* **2013**, *22*, 2873–2884. [[CrossRef](#)]

33. Sugiura, Y.; Makita, Y. Sodium Induces Octacalcium Phosphate Formation and Enhances Its Layer Structure by Affecting the Hydrated Layer Phosphate. *Cryst. Growth Des.* **2018**, *18*, 6165–6171. [[CrossRef](#)]
34. Sugiura, Y.; Makita, Y. Ammonium Substitutional Solid Solution of Octacalcium Phosphate (OCP). *Chem. Lett.* **2018**, *47*, 1371–1374. [[CrossRef](#)]
35. López-Macipe, A.; Gómez-Morales, J.; Rodríguez-Clemente, R. Nanosized hydroxyapatite precipitation from homogeneous calcium/citrate/phosphate solutions using microwave and conventional heating. *Adv. Mater.* **1998**, *10*, 49–53. [[CrossRef](#)]
36. Torrent-Burgués, J.; Gómez-Morales, J.; López-Macipe, A.; Rodríguez-Clemente, R. Continuous precipitation of hydroxyapatite from Ca/citrate/phosphate solutions using microwave heating. *Cryst. Res. Technol.* **1999**, *34*, 757–762. [[CrossRef](#)]
37. Riaz, T.; Zeeshan, R.; Zarif, F.; Ilyas, K.; Muhammad, N.; Safi, S.Z.; Rahim, A.; Rizvi, S.A.A.; Rehman, I.U. FTIR analysis of natural and synthetic collagen. *Appl. Spectrosc. Rev.* **2018**, *53*, 703–746. [[CrossRef](#)]
38. Bi, X.; Li, G.; Doty, S.B.; Camacho, N.P. A novel method for determination of collagen orientation in cartilage by Fourier transform infrared imaging spectroscopy (FT-IRIS). *Osteoarthr. Cartil.* **2005**, *13*, 1050–1058. [[CrossRef](#)] [[PubMed](#)]
39. Lakshmana, B.R. Infrared Absorption spectrum of sodium citrate. *J. Indian Inst. Sci.* **1957**, *39A*, 27–29.
40. Socrates, G. *Infrared and Raman Characteristics Group Frequencies: Tables and Charts*, 3rd ed.; John Wiley and Sons, Ltd.: Chichester, UK, 2001.
41. Nguyen, T.T.; Gobinet, C.; Lakshmana, B.R.; Feru, J.; Brassart-Pasco, S.; Manfait, M.; Piot, O. Characterization of type I and IV collagens by Raman microspectroscopy: identification of spectral markers of the dermo-epidermal junction. *Spectrosc. Int. J.* **2012**, *27*, 421–427. [[CrossRef](#)]
42. Chatzipanagis, K.; Iafisco, M.; Roncal-Herrero, T.; Bilton, M.; Tampieri, A.; Kröger, R.; Delgado-López, J.M. Crystallization of citrate-stabilized amorphous calcium phosphate to nanocrystalline apatite: A surface-mediated transformation. *CrystEngComm* **2016**, *18*, 3170–3173. [[CrossRef](#)]
43. Long, C. (Ed.) *Biochemists' Handbook*; Spon: London, UK, 1971.
44. López-Macipe, A.; Gómez-Morales, J.; Rodríguez Clemente, R. The Role of pH in the Adsorption of Citrate Ions on Hydroxyapatite. *J. Colloid Interface Sci.* **1998**, *200*, 114–120. [[CrossRef](#)]
45. Hemmilä, I.; Dakubu, S.; Mikkala, V.-M.; Siitara, H.; Lövgren, T. Europium as a label in time-resolved immunofluorometric assays. *Anal. Biochem.* **1984**, *137*, 335–343. [[CrossRef](#)]
46. Siqueira, K.P.F.; Lima, P.P.; Ferreira, R.A.S.; Carlos, L.D.; Bittar, E.M.; Matinaga, F.M.; Paniago, R.; Krambrock, K.; Moreira, R.L.; Dias, A. Influence of the Matrix on the Red Emission in Europium Self-Activated Orthoceramics. *J. Phys. Chem. C* **2015**, *119*, 17825–17835. [[CrossRef](#)]
47. Siqueira, K.P.F.; Lima, P.P.; Ferreira, R.A.S.; Carlos, R.D.; Bittar, E.M.; Granado, E.; González, J.C.; Abelenda, A.; Moreira, R.L.; Dias, A. Lanthanide Orthoantimonate Light Emitters: Structural, Vibrational, and Optical Properties. *Chem. Mater.* **2014**, *26*, 6351–6360. [[CrossRef](#)]
48. Richardson, F.S. Terbium(III) and europium(III) ions as luminescent probes and stains for biomolecular systems. *Chem. Rev.* **1982**, *82*, 541–552. [[CrossRef](#)]
49. Huang, R.H.; Huang, P.R.H. Phosphorescence of five amino acids. *Prog. Biochem. Biophys.* **1997**, *24*, 60–63.
50. Ward, J.L.; Walden, G.L.; Winefordner, J.D. A review of recent uses of phosphorimetry for organic analysis. *Talanta* **1981**, *28*, 201–206. [[CrossRef](#)]
51. Zollfrank, C.; Scheel, H.; Brungs, S.; Greil, P. Europium(III) Orthophosphates: Synthesis, characterization, and optical properties. *Cryst. Growth Des.* **2008**, *8*, 766–770. [[CrossRef](#)]
52. Lakowicz, J.R. *Principles of Fluorescence Spectroscopy*, 2nd ed.; Kluwer Academic/Plenum Publishers: New York, NY, USA, 1999; pp. 130–131. ISBN 978-0-387-46312-4.
53. ISO 10993-5:2009. Biological Evaluation of Medical Devices—Part 5: Tests for In Vitro Cytotoxicity. Available online: <https://www.iso.org/standard/36406.html> (accessed on 22 December 2018).

